Tectonophysics 664 (2015) 176–181

Contents lists available at ScienceDirect

Tectonophysics

journal homepage: www.elsevier.com/locate/tecto

Lg attenuation tomographic models of Himalaya and southern Tibet

Chandrani Singh [a,*], Pushkar Mondal [a], Sagar Singh [a], Debasis D. Mohanty [a], Namrata Jaiswal [a], M. Ravi Kumar [b]

[a] Department of Geology and Geophysics, Indian Institute of Technology Kharagpur, West Bengal 721302, India
[b] National Geophysical Research Institute, CSIR, Hyderabad 500007, India

ARTICLE INFO

Article history:
Received 9 June 2015
Received in revised form 9 September 2015
Accepted 11 September 2015
Available online 26 September 2015

Keywords:
Lg wave
Attenuation tomography
Intrinsic and scattering effects
Himalaya and southern Tibet

ABSTRACT

We investigate the *Lg* attenuation structure of the crust beneath the tectonically complex Himalaya and southern Tibet regions adopting a tomographic regionalization method. A total of 1671 earthquake waveforms registered at 38 seismic stations operated in the region are selected for the initial *LgQ* measurements using the standard two-station method. Q_0 (1 Hz *LgQ*) values of 76 high quality interstation paths are finally considered as input for the tomographic inversion. The estimates of Q_0 exhibit distinct variations in the crustal attenuation from north to south across the whole region. The zones of lowest Q_0 values (<50) are observed along the Main Central Thrust (MCT) in Sikkim, Lesser Himalaya and some parts of the Greater Himalaya. Southern Tibet is characterized by low Q_0 (< 100) values. These observations are consistent with the results of body wave attenuation and velocity structure reported for the region. We interpret the variations in the attenuation characteristics in terms of both the intrinsic and scattering contributions caused by thermal effects, presence of aqueous fluids as well as heterogeneities present below these seismically active regions. Our results are found to be comparable with the other parts of Himalaya and Tibet.

1. Introduction

Lg is typically the most notable phase observed with the largest amplitude on regional (>200 km) short period seismograms. It travels predominantly through the continental crust within a group velocity window of 3.6 and 2.8 km/s in the frequency range of 0.2–5 Hz. The wavetrain is a summation of higher-mode surface waves propagating in the crustal waveguide, or multiply reflected *S* waves bouncing supercritically between the free surface and the Moho discontinuity (Knopoff et al., 1973). The amplitude of *Lg* wave is sensitive to their propagation in different tectonic structures like faults, mountains and ocean basins. A detailed information regarding the spatial variations in *Lg* wave propagation is required for assessing strong ground motion due to earthquakes and for mitigation of seismic hazard (Furumura et al., 2014). The group velocity and quality factor (*Q*, which is inversely proportional to attenuation coefficient) of *Lg* waves reflect average values within the crust. The *LgQ* estimates are often frequency dependent and assumed to obey a power law:

$$Q_{Lg}(f) = Q_0 f^{\eta} \quad (1)$$

where Q_0 is *LgQ* at 1 Hz and and η denotes its frequency dependence. Many factors such as complexities in the crustal structure along the propagation path, localized small-scale heterogeneities, attenuation or unusual velocity structure in the crust, restrict its propagation, resulting in weak or no *Lg* arrivals on a seismogram (Ruzaikin et al., 1977; Ni and Barazangi, 1983; Fan and Lay, 2002; Xie et al., 2004; Aleqabi and Wysession, 2006). LgQ_0 is seen to be highly variable by up to an order of magnitude, across major continents (Xie et al., 2004, 2006)]. Such large variations are caused due to the fact that attenuation is strongly affected by crustal properties such as partial melting, fluid content and temperature, which can vary significantly from one region to another (Mitchell et al., 1997). Also, it is observed that the *LgQ* value correlates well with the intensity of recent tectonic activity in the crust (Mitchell, 1995). It exhibits higher values for stable regions in contrast to lower values in tectonically active regions (Singh et al., 2011, 2012). The attenuation appertains to either strong small-scale scattering/heterogeneity or partial melting in the tectonically deformed crust (Fan and Lay, 2003a). Therefore attenuation tomography is very useful for identifying the physical state of the crust underlying a region.

Our area of present study encompasses the tectonically complex Himalaya and southern Tibet region (Fig. 1). This is a crucial region to understand the process of continental collision between the Indian and Eurasian plates. The ongoing collision has created the Himalaya and Tibetan plateau through a series of deformational processes. The collision is the dominant force behind the rise of the Himalayan mountain range and the uplift of the Tibetan plateau. The recent episode emanated about 55 Ma ago. It is opined that the Indus Tsangpo Suture Zone (ITSZ) represents a surface trace that resulted due to the collision of the Indian shield with the Lhasa terrane of southern Tibet. This collision zone hosts numerous tectonostratigraphic units such as the main central thrust (MCT), main boundary thrust (MBT) and the main frontal thrust (MFT) (Hodges, 2000) and served as northern and southern

* Corresponding author.
E-mail address: chandrani@gg.iitkgp.ernet.in (C. Singh).

http://dx.doi.org/10.1016/j.tecto.2015.09.009
0040-1951/

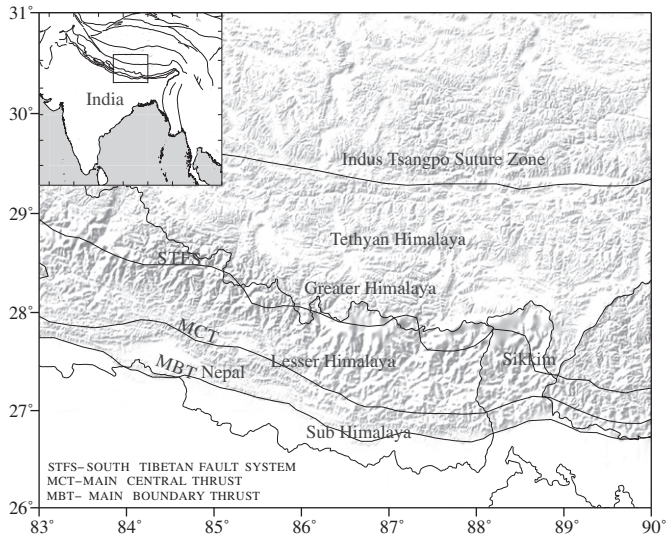

Fig. 1. Tectonic map of our study area that includes parts of Tibet and the Himalaya (modified after Monsalve et al., 2008). Inset shows the location of the study area with respect to India.

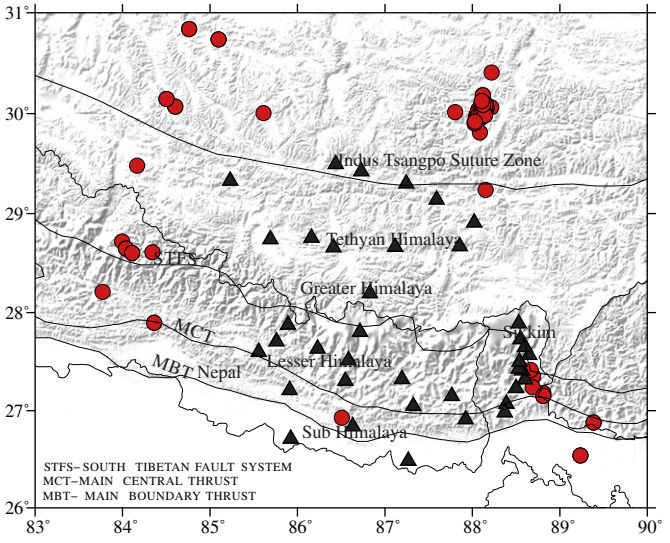

Fig. 2. Locations of the earthquakes (circles) and stations (triangles) used in this study.

boundary of different Himalayas, e.g., in southern Nepal, MFT limits the northern boundary of the Indo-Gangetic plains; the Sub-Himalayan Zone is located between MFT and MBT; the Lesser Himalaya lies north of the MBT and its northern boundary is limited by the MCT; north of MCT is the Greater Himalayan zone; the South Tibetan Fault Zone separates the Greater Himalaya from the Tethyan Himalaya to the North; the Indus-Tsanpo Suture Zone (ITSZ) represents the northern limit of the Tethyan Himalaya. The region is also seismically very active and experiences a large number of earthquakes every year. Recently, on 25th April, 2015, the Nepal Himalayan sector (lat 28.147°N; long 84.708°E) is rocked by a devastating earthquake of M_w 7.8 (USGS). High-strain accumulation due to continent-continent collision between Indian and Eurasian plates along the different Himalayan frontal thrusts results in the occurrence of these earthquakes.

Several attenuation measurements have been performed for the Tibetan plateau using recent broad band *Lg* data (Fan and Lay, 2002, 2003a,2003b; Xie, 2002; Xie et al., 2006; Bao et al., 2011; Singh et al., 2012; Zhao et al., 2013). The results broadly suggest widespread partial melting or channel flow exists in the crust along certain pockets within the plateau. In the present study, we develop a tomographic image of *Lg* attenuation in order to enhance the understanding of *Lg* wave propagation through the crust of Himalaya and southern Tibet. We attempt to present the tectonic implications of the variations in attenuation structure and its relation to the physical state of the crust. We also employ the other complementary information to gain a detailed insights into the mechanisms of attenuation.

2. Data

The *Lg* data set used in the present study consists of waveforms of 1585 earthquakes recorded by a 27 station broadband seismic network (HIMNT) operated in eastern Nepal and southern Tibet during 2001–2003 with a station spacing of ~40–50 km (Monsalve et al., 2006). These data are complemented by another data set of 86 events recorded by 11 seismic stations deployed along a 110 km profile in the Sikkim Himalaya during the years 2004-2010 (Fig. 2). A total of 1068 pairs of high quality interstation paths enabled us to employ the standard two-station method for LgQ estimation. We used only the crustal earthquakes which are recorded by most of the stations. Waveforms with a good signal-to-noise (S/N) ratio are analyzed to ensure reliable results. The 1 Hz *LgQ* (Q_0) values are measured between many pairs of stations and input to a back-projection algorithm to obtain laterally varying Q_0 models.

3. Methodology

3.1. Two-station method

Denoting the two stations as *i* and *j* at which the *Lg* amplitude spectra $A_i(f)$ and $A_i(f)$ at frequency *f* can be collected, the scaled spectral ratio can be defined as (Xie et al., 2004)

$$R(f) = \left(\Delta_i^{1/2}/\Delta_j^{1/2}\right)\left[A_i(f)/A_j(f)\right] \tag{2}$$

where Δ_i and Δ_j are the epicentral distances. The square root of their ratio cancels the effect of geometrical spreading in 1D. Assuming that the *Lg*Q follows the power-law frequency dependence (Eq. (1)), the Q_0 and η over the interstation path $\Delta_{i,j}$ can be estimated as

$$\ln\left[\frac{V_{Lg}}{\pi\Delta_{i,j}}\ln\left(\frac{\Delta_i^{1/2}}{\Delta_j^{1/2}}\times\frac{A_i(f)}{A_j(f)}\right)\right] = (1-\eta)\ln f - \ln Q_0 \tag{3}$$

where V_{Lg} is the typical *Lg* velocity of 3.5 km/s. The left hand side is denoted as "reduced spectral ratio." The instrument corrected vertical component *Lg* waveforms are used. An example of a typical seismogram is shown in Fig. 3.

By taking the ratio of *Lg* spectra from the same source and using the square root of the ratio of their epicentral distances, this method eliminates the effects of source and geometrical spreading respectively. The method was also used earlier for the *Lg* attenuation studies in the Himalyan collision zone (Xie et al., 2004; Ashish et al., 2009; Singh et al., 2012). While the computation of Q_0 is stable, the measurement of stable interstation η is difficult (Xie et al., 2004). So we focus on the attenuation factor Q_0.

After applying the waveform selection criterion to over initial data, we accept the spectra from two stations that are (1) aligned approximately with the source and (2) separated enough to qualify the use of standard two-station method for *LgQ* estimation (Xie et al., 2004). In an ideal situation, the two-station method presumes that the recording stations are aligned exactly with the source, but in a real scenario, a perfect alignment of stations and source is usually not possible (Xie et al., 2004). To define the alignment, an angle $\delta\theta$, which is the difference between the azimuths from the source and the two stations, is introduced (for more details, see Xie et al. (2004). In the present study following Xie et al. (2004), we limit $\delta\theta$ to 15° to reduce the error. The other crucial parameter is the interstation distance $\Delta_{i,j}$, which can cause a potential error and is associated to the obtained Q_0 value on the corresponding

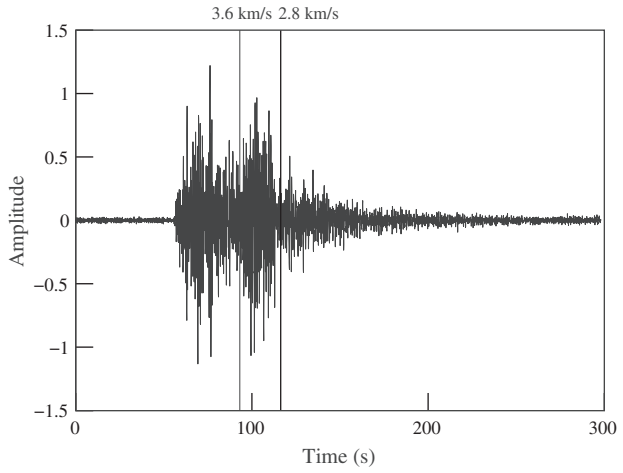

Fig. 3. Example seismogram (vertical component) of an event that occurred on 16 June 2002 at 20 h, 35 min and 42 s recorded at RUMJ station located in Lesser Himalaya. Vertical lines limit the *Lg* group–velocity window (2.8–3.6 km/s).

path. Initially, all possible pairs of two stations are used to estimate the interstation spectral ratios, regardless of the interstation distance $\Delta_{i,j}$. Thereafter, the error in the estimated interstation Q_0 caused by $\Delta_{i,j}$ is obtained using the following equation given by Xie et al. (2004)

$$\frac{\delta Q_0}{Q_0} \approx 1.1\left(\frac{Q_0}{\Delta_{i,j}}\right)\delta x \tag{4}$$

To keep this error lower than 25% with a given error in δx as 0.2, the interstation ratio between Q_0 and $\Delta_{i,j}$ should not be greater than 1.14. Zor et al. (2007) have considered this ratio as 1.6 by keeping the error lower than 35%. However, by applying the aforementioned criterion (error lower than 25%) to the initial pairs, we found 76 pairs of spectra and used them as inputs for the tomographic inversion.

3.2. Tomography

3.2.1. Back-projection algorithm

To create a tomographic image of the Q_0 estimates in the region of interest, we used the well established back-projection tomographic method (Xie and Mitchell, 1990). The method presumes that the area covered by the scattered *Lg* wave energy can be approximated by an ellipse with the source at one focus and the seismic station at the other. It converges fast and needs minimal computer storage (for more details, see Xie and Mitchell, 1990). To apply this method we divided the whole area into several grids such that the grid size is adequate to achieve proper resolution. We have considered the grid size as $0.05^\circ \times 0.05^\circ$ in the present study. The input data contains the Q_0 value for each station pair. Several ellipses with major and minor axes are considered as a function of the distance between the station pair and the center of each ellipse is assumed to be the midpoint of the corresponding station pair. The major and minor axes of the ellipses are such that they cover the area adequately. Thereafter, the average value of quality factor over each ellipse (corresponding to a station pair) is assigned as the average of quality factor between the station pair. By implementing the back-projection algorithm, we have calculated the Q for every grid by using the knowledge of Q distribution over each ellipse (Fig. 4) according to

$$\frac{1}{Q_n} = \frac{1}{S_n}\sum_{m=1}^{N_g}\frac{S_{mn}}{Q_m} + \epsilon_n \tag{5}$$

where $n = 1, 2, 3....N_d$, N_d is the total number of seismic records, N_g is the number of grids considered, Q_n is the average quality factor associated

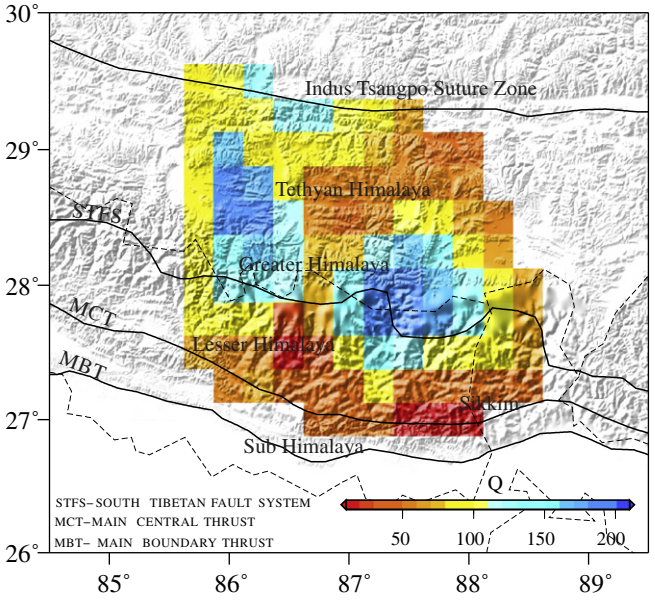

Fig. 4. Tomographic image of LgQ_0 obtained in the present study.

with nth ellipse, Q_m is the quality factor for each grid, S_{mn} is the area of superposition between mth grid and nth ellipse, ϵ_n represents error corresponding to iteration over the nth ellipse and S_n is the area of the nth ellipse defined by

$$S_n = \sum_{j=1}^{N_g} S_{jn} \tag{6}$$

3.3. Error and resolution analysis

In the back-projection tomographic method, the resolution is assessed using the *point spreading functions* (PSF) (Humphreys and Clayton, 1988). This is estimated by considering a model in which we assign Q^{-1} as unity in a single cell within the area of interest and zero everywhere else. Fig. 5 illustrates the PSF values for two selected cells, which shows the potential to resolve the features in the region. We calculated the error corresponding to each iteration by observing its nature while implementing the back-projection algorithm (Fig. 6). We observed that during the initial stage, the error peaks up to 100%, but as the number of iterations increase, the error starts decreasing. However,

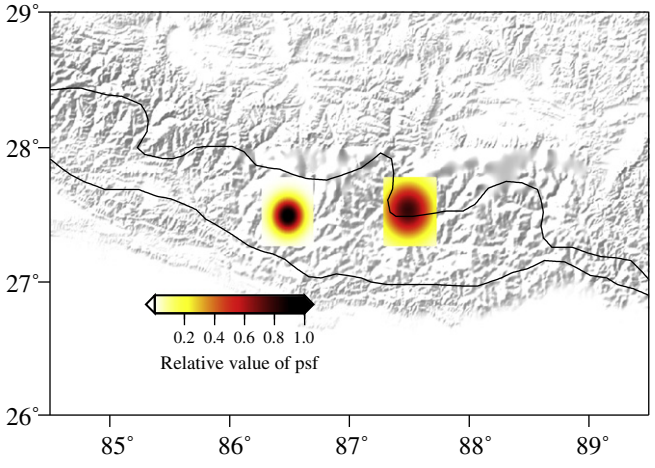

Fig. 5. Point spreading functions (PSF's) for two selected cells.

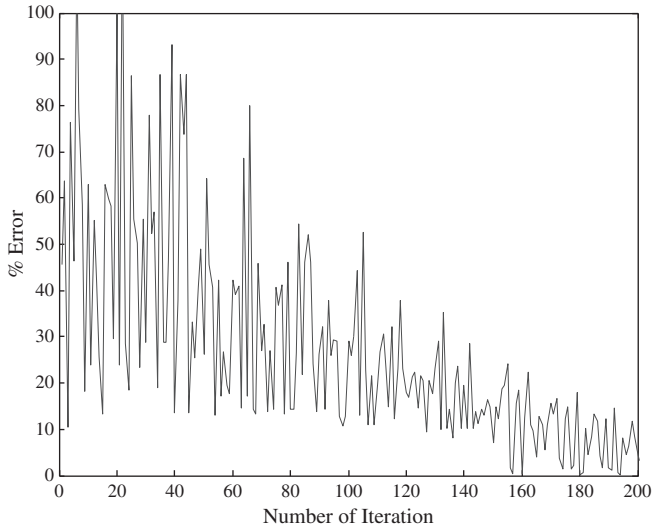

Fig. 6. Estimated error (%) corresponding to each step of iteration during the inversion for LgQ_0 using the back-projection tomography method.

due to the substantial increase in computing time, the iteration is accomplished with an average 10–20% error. As the spatial dimension of the area is small, the model resolution is expected to be higher.

4. Results and discussion

4.1. Spatial variations of Q_0 and mechanisms contributing to attenuation

A high spatial resolution map of *Lg* attenuation (Fig. 4) is achieved through 76 pairs of spectra obtained from waveforms recorded by dense networks operated in the Himalaya and southern Tibet regions. We observed distinct variations in crustal attenuation from north to south across the regions. The region is tectonically very complex and seismically very active due to the high-strain accumulation caused by the continent-continent collision between the Indian and Eurasian plates. The lateral variations in *Q* are consistent with the tectonic features of the area. The lowest Q_0 values (<50) are observed along MCT in Sikkim and Lesser Himalayas and in some parts of Greater Himalaya. Southern Tibet is characterized by low Q_0 (<100).

The attenuation of *Lg* and its correlation with large scale crustal features has been described by numerous authors including Kennett (1986), Mitchell and Hwang (1987), Bowman and Kennett (1991), Campillo and Plantet (1991), Mitchell et al. (1998) and Baumgardt (2001). These studies demonstrate that *Lg* wave attenuation is strongly correlated with the age of the crust, variations in crustal thickness, the nature of the crust–mantle transition, sediment thickness and crustal complexity. The *LgQ* variation can reflect the physical properties of the crust. It also helps to geophysically mark the major terrane boundaries (Gallegos et al., 2014). Zhao et al. (2013) have suggested that strong thermal activities and heterogeneities caused due to the partially molten magma chambers beneath the Tibetan Plateau are responsible for both the intrinsic and scattering attenuation to be effective in the underlying medium. In the Garwhal–Kumaun Himalayan segment (west of Nepal Himalaya), Mukhopadhyay et al. (2010) have observed the higher scattering attenuation in the crust. MCT is one of the major tectonostratigraphic units in the Himalaya and accommodated significant amounts of convergence between India and Eurasia, and hence prominent zones of very low Q_0 along MCT may reflect the high structural heterogeneity. The medium below Sikkim Himalaya is highly heterogeneous in nature (Singh et al., 2010), which is corroborated by the high attenuation of *Lg* waves in the crust. In southern Tibet, Singh et al. (2015a) (unpublished work) have observed the predominance of intrinsic absorption over scattering attenuation. Large variation in heat-flow measurements over a short distance is apparent in southernmost Tibet, and the heat anomaly is of shallow origin (no greater than 25 km)(Francheteau et al., 1984). According to Zhao et al. (2013), the rugged topography, double thick crust and weak Moho signature below a major portion of the Tibetan plateau restricts the propagation of *Lg* as a guided wave. Low scattering *Q* due to strong small-scale structural heterogeneities within the Tibetan crust might also have contributed to the observed low *LgQ* (Singh et al., 2012). Sheehan et al. (2014) have observed high body waves attenuation within the crust of southern Tibetan Plateau compared to the crust beneath the Lesser Himalaya and Ganges Plain. This observation is interpreted in terms of presence of warm, felsic material in the middle and upper crust of the southern Tibetan Plateau, similar to the other parts of Himalaya (Yin and Harrison, 2000). Therefore, the low Q_0 (< 100) value in southern Tibet may originate from both intrinsic and scattering effects.

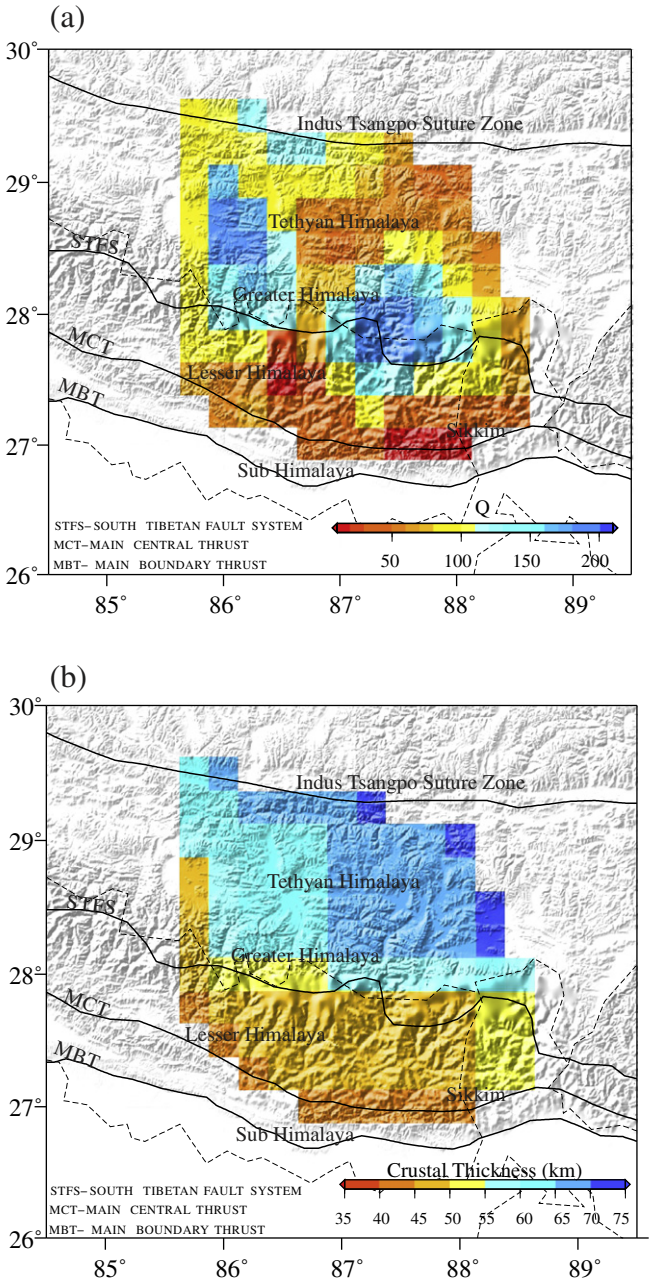

Fig. 7. Comparison of (a) LgQ_0 obtained in the present study with (b) estimated crustal thickness map for the region from CRUST1.0 model (Laske et al., 2013).

Fig. 7 shows a comparison of our *LgQ* model with the crustal thickness map of the area derived from CRUST1.0 model (Laske et al., 2013). Zhao et al. (2010)) and Zhao et al. (2013) have observed a trend that relates high *LgQ* with a thicker crust. Results from our study do not reveal any significant correlation except in some parts of the higher Himalaya where high *LgQ* is associated with a thicker crust. The Southern Tibetan plateau, which exhibits low *LgQ* values, is characterized by thick crust (Singh et al., 2015b). Zhao et al. (2013) suggested that the *Lg* attenuation features of Tibetan plateau are quite uncommon and should not be fit into a standard crust model.

Fig. 8 represents a cartoon summarizing our 2D *LgQ* model from south to north across the study region including the velocity and body wave attenuation structure proposed for the region (modified after Monsalve et al., 2008). The two low Q_0 pockets in the present study correlate well with the low Q_p and Q_s below lesser Himalaya and southern Tibet (Sheehan et al., 2014) and coincide with low $\frac{V_p}{V_s}$ zones observed from a tomography study (Monsalve et al., 2008). High electrical conductivity is also observed beneath the lesser Himalaya (Unsworth et al., 2005). All the observations along with our results collectively indicate possible presence of significant amounts of fluids trapped in the crust, since seismic waves are strongly attenuated by a fluid layer. However, Xie et al. (2004) have interpreted that the aqueous fluid trapped in the upper crust and a mid crustal partial melting zone caused due to the underthrusting of the Indian lithosphere probably explains the higher *Lg* attenuation observed in southern Tibet area.

4.2. Comparison of the results with the previous studies in the Himalaya–Tibet collision zone.

Several works reported low Q_0 values in the Himalaya–Tibet collision zone. Very low Q_0 values in the range of 30–60 are reported by Ashish et al. (2009) for High Himalaya. Fan and Lay (2003a) have estimated a $Q_0 = 106 \pm 18$ for eastern Tibet whereas Xie (2002) reported $Q_0 = 126 \pm 9$. Further, Fan and Lay (2002)) and Fan and Lay (2003b) obtained $Q_0 = 100 \pm 20$ and $Q_0 = 83 \pm 19$ for the same region respectively. A low value of $Q_0 = 79 \pm 4$ is estimated for northern central Tibet (Fan and Lay, 2003a). In central Tibet a persistent and nearly constant value of ≈ 90 is observed along the INDEPTH III profile (Xie et al., 2004). Subsequently, the consistent low Q_0 values along the Hi-CLIMB profile is also observed (Singh et al., 2012) that manifests the presence of omnipresent partial melting of the crust throughout the plateau. Zhao et al. (2013) have reported high seismic wave attenuation structure in the crust and upper mantle of the northern Tibetan Plateau. Hence the present results are consistent with the other reports of *LgQ* values in Himalaya and Tibet.

5. Conclusions

Based on the data from regional *Lg* waves collected from 38 seismic stations operated at Himalaya and southern Tibet, a tomographic attenuation model is obtained for the region. We find a spatial variation of *LgQ* values across different sectors of the region due to the differences in the crustal character of the underlying medium. The spatial variations in *Q* are consistent with the tectonic features of the area. We observed the lowest Q_0 values along MCT in Sikkim and Lesser Himalayas and along some pockets of Greater Himalaya, which may be corroborated by the high attenuation of *Lg* wave in the crust due to its highly heterogeneous structure. Low Q_0 values in Southern Tibet may be caused due to the intrinsic and scattering effects resulting from thermal activities, presence of aqueous fluids and strong small-scale structural heterogeneities present in the crust.

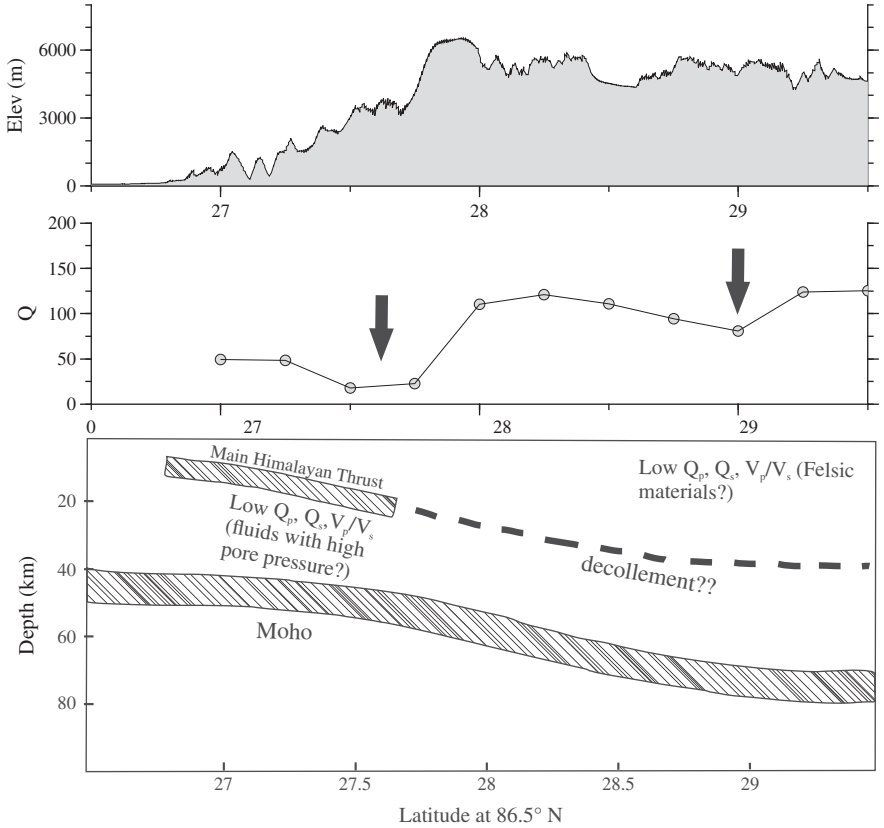

Fig. 8. A cartoon depicting the 2D–*LgQ* model from south to north across the region (modified after (Monsalve et al., 2008) together with the velocity and body wave attenuation structure.

Acknowledgments

We acknowledge IRIS DMC (http://ds.iris.edu/ds/nodes/dmc) and Project Team of HIMNT experiment for making seismic data available. We thank both the reviewers of this manuscript for their valuable suggestions. This study has been supported by a grant from the Ministry of Earth Sciences (MoES), IITKGP/IAI.

References

Aleqabi, G.I., Wysession, M.E., 2006. QLg distribution in the basin and range province of the Western United States. Bull. Seismol. Soc. Am. 96, 348–354.
Ashish, Padhi, A., Rai, S.S., Gupta, S., 2009. Seismological evidence for shallow crustal melt beneath the Garhwal High Himalaya, India: implications for the Himalayan channel flow. Geophys. J. Int. 177, 1111–1120.
Bao, X., Sandvol, E., Ni, J., Hearn, T., Chen, Y.J., Shen, Y., 2011. High resolution regional seismic attenuation tomography in eastern Tibetan Plateau and adjacent regions. Geophys. Res. Lett. 38, l16304.
Baumgardt, D.R., 2001. Sedimentary basins and the blockage of Lg wave propagation in the continents. Pure Appl. Geophys. 158, 1207–1250.
Bowman, J.R., Kennett, B.L.N., 1991. Propagation of Lg waves in the North Australian Craton: influence of crustal velocity gradients. Bull. Seismol. Soc. Am. 81, 592–610.
Campillo, M., Plantet, J., 1991. Frequency dependence and spatial distribution of seismic attenuation in France: experimental results and possible interpretations. Phys. Earth Planet. Inter. 67, 48–64.
Fan, G., Lay, T., 2002. Characteristics of Lg attenuation in the Tibetan Plateau. J. Geophys. Res. 107 (ESE 14–1–ESE 14–15, 2256).
Fan, G.-W., Lay, T., 2003a. Strong Lg wave attenuation in the Northern and Eastern Tibetan Plateau measured by a two-station/two-event stacking method. Geophys. Res. Lett. 30, 1530.
Fan, G.-W., Lay, T., 2003b. Strong Lg attenuation in the Tibetan Plateau. Bull. Seismol. Soc. Am. 93, 2264–2272.
Francheteau, J., Jaupart, C., Jie, S.X., Wen-Hua, K., De-Lu, L., Jia-Chi, B., Hung-Pin, W., Hsia-Yeu, D., 1984. High heat flow in southern Tibet. Nature 307, 32–36.
Furumura, T., Hong, T.-K., Kennett, B., 2014. Lg wave propagation in the area around Japan: observations and simulations. Prog. Earth Planet. Sci. 1.
Gallegos, A., Ranasinghe, N., Ni, J., Sandvol, E., 2014. Lg attenuation in the central and eastern United States as revealed by the EarthScope Transportable Array. Earth Planet. Sci. Lett. 402, 187–196 (special issue on {USArray} science).
Hodges, K.V., 2000. Tectonics of the Himalaya and southern Tibet from two perspectives. Geol. Soc. Am. Bull. 112, 324–350.
Humphreys, E., Clayton, R.W., 1988. Adaptation of back projection tomography to seismic travel time problems. J. Geophys. Res. 93, 1073–1085.
Kennett, B.L.N., 1986. Lg waves and structural boundaries. Bull. Seismol. Soc. Am. 76, 1133–1141.
Knopoff, L., Schwab, F., Kauselt, E., 1973. Interpretation of Lg*. Geophys. J. R. Astron. Soc. 33, 389–404.
Laske, G., Masters, G., Ma, Z., Pasyanos, M., 2013. Update on CRUST1.0—a 1-degree global model of Earth's crust. EGU General Assembly Conference Abstracts, vol. 15 of EGU General Assembly Conference Abstracts, p. 2658.
Mitchell, B.J., 1995. Anelastic structure and evolution of the continental crust and upper mantle from seismic surface wave attenuation. Rev. Geophys. 33, 441–462.
Mitchell, B.J., Hwang, H.J., 1987. Effect of low Q sediments and crustal Q on Lg attenuation in the United States. Bull. Seismol. Soc. Am. 77, 1197–1210.
Mitchell, B.J., Pan, Y., Xie, J., Cong, L., 1997. Lg coda Q variation across Eurasia and its relation to crustal evolution. J. Geophys. Res. 102, 22,767–22,779.
Mitchell, B.J., Baqer, S., Akinci, A., Cong, L., 1998. Lg Coda Q in Australia and its relation to crustal structure and evolution. Pure Appl. Geophys. 153, 639–653.
Monsalve, G., Sheehan, A., Schulte-Pelkum, V., Rajaure, S., Pandey, M.R., Wu, F., 2006. Seismicity and one-dimensional velocity structure of the Himalayan collision zone: earthquakes in the crust and upper mantle. J. Geophys. Res. 111.
Monsalve, G., Sheehan, A., Rowe, C., Rajaure, S., 2008. Seismic structure of the crust and the upper mantle beneath the himalayas: evidence for eclogitization of lower crustal rocks in the indian plate. J. Geophys. Res. 113.
Mukhopadhyay, S., Sharma, J., Del-Pezzo, E., Kumar, N., 2010. Study of attenuation mechanism for Garwhal–Kumaun Himalayas from analysis of coda of local earthquakes. Phys. Earth Planet. Inter. 180, 7–15.
Ni, J., Barazangi, M., 1983. High-frequency seismic wave propagation beneath the Indian Shield, Himalayan Arc, Tibetan Plateau and surrounding regions: high uppermost mantle velocities and efficient Sn propagation beneath Tibet. Geophys. J. R. Astron. Soc. 72, 665–689.
Ruzaikin, A.I., Nersesov, I.L., Khalturin, V.I., Molnar, P., 1977. Propagation of Lg and lateral variations in crustal structure in Asia. J. Geophys. Res. 82, 307–316.
Sheehan, A.F., de la Torre, T.L., Monsalve, G., Abers, G.A., Hacker, B.R., 2014. Physical state of Himalayan crust and uppermost mantle: constraints from seismic attenuation and velocity tomography. J. Geophys. Res. 119, 567–580.
Singh, A., Kumar, M.R., Raju, P.S., 2010. Seismic structure of the underthrusting indian crust in Sikkim Himalaya. Tectonics 29, TC6021.
Singh, C., Singh, A., Mukhopadhyay, S., Shekar, M., Chadha, R.K., 2011. Lg attenuation characteristics across the Indian Shield. Bull. Seismol. Soc. Am. 101, 2561–2567.
Singh, C., Shekar, M., Singh, A., Chadha, R.K., 2012. Seismic attenuation characteristics along the Hi–CLIMB profile in Tibet from Lg Q inversion. Bull. Seismol. Soc. Am. 102, 783–789.
Singh, A., Singh, C., Kennett, B., 2015a. A review of crust and upper mantle structure beneath the Indian subcontinent. Tectonophysics 644–645, 1–21.
Singh, S., C. Singh, S. Mukhopadhyay, and H. Sahu, Attenuation characteristics in eastern Himalaya and southern Tibetan Plateau: an understanding of the physical state of the medium, *unpublished work*, 2015b
Unsworth, M.J., Jones, A.G., Wei, W., Marquis, G., Gokarn, S.G., Spratt, J.E., 2005. Crustal rheology of the Himalaya and Southern Tibet inferred from magnetotelluric data. Nature 438, 78–81.
Xie, J., 2002. Lg Q in the Eastern Tibetan Plateau. Bull. Seismol. Soc. Am. 92, 871–876.
Xie, J., Mitchell, B.J., 1990. A back-projection method for imaging large-scale lateral variations of Lg Coda Q with application to continental Africa. Geophys. J. Int. 100, 161–181.
Xie, J., Gok, R., Ni, J., Aoki, Y., 2004. Lateral variations of crustal seismic attenuation along the INDEPTH profiles in tibet from Lg Q inversion. J. Geophys. Res. 109, b10308.
Xie, J., Wu, Z., Liu, R., Schaff, D., Liu, Y., Liang, J., 2006. Tomographic regionalization of crustal Lg Q in eastern Eurasia. Geophys. Res. Lett. 33, l03315.
Yin, A., Harrison, T.M., 2000. Geologic evolution of the Himalayan–Tibetan orogen. Annu. Rev. Earth Planet. Sci. 28, 211–280.
Zhao, L.-F., Xie, X.-B., Wang, W.-M., Zhang, J.-H., Yao, Z.-X., 2010. Seismic Lg-wave Q tomography in and around Northeast China. J. Geophys. Res. 115.
Zhao, L.-F., Xie, X.-B., He, J.-K., Tian, X., Yao, Z.-X., 2013. Crustal flow pattern beneath the Tibetan Plateau constrained by regional Lg-wave Q tomography. Earth Planet. Sci. Lett. 383, 113–122.
Zor, E., Sandvol, E., Xie, J., Trkelli, N., Mitchell, B., Gasanov, A.H., Yetirmishli, G., 2007. Crustal attenuation within the Turkish Plateau and surrounding regions. Bull. Seismol. Soc. Am. 97, 151–161.